Received: 5 May 2019 | Revised: 8 August 2019 | Accepted: 15 August 2019

DOI: 10.1111/ina.12597

ORIGINAL ARTICLE

WILEY

Quantification of the impact of cooking processes on indoor concentrations of volatile organic species and primary and secondary organic aerosols

Felix Klein | Urs Baltensperger | André S. H. Prévôt | Imad El Haddad

Laboratory of Atmospheric Chemistry, Paul Scherrer Institute, Villigen, Switzerland

Correspondence
Imad El Haddad and Felix Klein, Laboratory of Atmospheric Chemistry, Paul Scherrer Institute, Villigen 5232, Switzerland.
Email: imad.el-haddad@psi.ch

Present address
Felix Klein, Meteorologisches Observatorium Hohenpeissenberg, Deutscher Wetterdienst (DWD), Hohenpeissenberg, Germany

Funding information
Swiss National Science Foundation (SNF)

Abstract

Cooking is recognized as an important source of particulate pollution in indoor and outdoor environments. We conducted more than 100 individual experiments to characterize the particulate and non-methane organic gas emissions from various cooking processes, their reaction rates, and their secondary organic aerosol yields. We used this emission data to develop a box model, for simulating the cooking emission concentrations in a typical European home and the indoor gas-phase reactions leading to secondary organic aerosol production. Our results suggest that about half of the indoor primary organic aerosol emission rates can be explained by cooking. Emission rates of larger and unsaturated aldehydes likely are dominated by cooking while the emission rates of terpenes are negligible. We found that cooking dominates the particulate and gas-phase air pollution in non-smoking European households exceeding 1000 μg m^{-3}. While frying processes are the main driver of aldehyde emissions, terpenes are mostly emitted due to the use of condiments. The secondary aerosol production is negligible with around 2 μg m^{-3}. Our results further show that ambient cooking organic aerosol concentrations can only be explained by super-polluters like restaurants. The model offers a comprehensive framework for identifying the main parameters controlling indoor gas- and particle-phase concentrations.

KEYWORDS
Cooking emissions, HR-TOF-AMS, Indoor air quality, POA, PTR-TOF-MS, SOA

1 | INTRODUCTION

In developed countries people spend on average about 16 hours per day indoor.[1] Indoor air can be heavily polluted with non-methane organic gases (NMOG)[2,3] or high particle loadings[4] posing a threat to the health of the inhabitants. While some studies suggest that the indoor air quality is mainly driven by regional outdoor pollution,[5] others argue that residential exposure to particle pollution far exceeds (eg, by 150%[6]) the exposure to particles from outdoor origins. Residential pollution exposure cannot be characterized by ambient measurements alone, and an accurate knowledge of indoor sources and loss processes is the key for assessing indoor air quality.

Cooking is already recognized as main source of indoor particulate air pollution in developed countries.[4,7] The processes used in cooking such as frying, roasting, grilling, boiling, and broiling contribute to particle emissions. The physical stirring of food has been

Imad El Haddad and Felix Klein are contributed equally.

found to lead to primary aerosol generation due to the splashing of the ingredients. The ingredient combustion during cooking can lead to direct emissions, and hot vapors in the cooking fumes from oil decomposition[8] may also cool and nucleate to form more particles. Other known indoor emission sources related to residential cooking are electrical and gas stoves emitting high amounts of small particles (<10 nm)[9] and nitrogen oxides.[10] While many of the ingredients and cooking methods are common to various culinary techniques, particle emission rates from cooking span several orders of magnitudes,[11,12] affected by ingredients, procedures (eg, boiling vs frying vs charbroiling), and cooking temperature. Cooking has been also identified as an important outdoor source of primary organic aerosols based on aerosol mass spectrometry measurements[13]; however, the processes dominating these emissions remain unclear.[14] Currently, there is an urgent need for a systematic assessment of the processes controlling the cooking emission rates, in order to constrain the contribution of these emissions to indoor and outdoor air quality.

In addition to particle emissions, cooking is known to generate significant amounts of vapors, comprising aldehydes from oil heating[15,16] or restaurant emissions.[17] Recent studies discovered that many cooking processes may constitute an important source of NMOG indoors including potentially harmful substances like aldehydes or terpenes.[18-20] Studies on sources of indoor gas-phase air pollution so far focused mostly on cleaning detergents and air fresheners (terpenes),[21] scented candles (carbonyls),[22] building materials (all classes of compounds),[23] or smoking.[24] Also recognized as an important source of NMOG indoors is the transfer of outdoor air pollution to the indoor.[25,26] However, how gas-phase cooking emission rates compare to those from other indoor and outdoor sources remains unclear. Besides the direct effect of NMOGs on human health,[27] they are also precursors of secondary organic aerosol (SOA) through their reactions with ozone or OH radicals.[28] Still not much is known about the production of SOA from most NMOG indoors. Most studies investigating SOA formation indoors focused on terpenoid reactions (mostly limonene from cleaning detergents) with ozone.[29-33] Two recent studies trying to model the SOA formation indoors from different NMOG also concluded that SOA formation is dominated by high terpene (mostly limonene) emissions from cleaning products.[34,35] However, all of these studies neglect the high amounts of various terpenes emitted from frying food with condiments [19] as well as the high amounts of aldehydes emitted by frying processes.[18,36,37]

Cooking-induced primary and secondary pollution is not only controlled by the cooked ingredients and cooking style or setting (fuel,[38] pan,[39] oil used, and cooking method[40]), but also depends on the air exchange rates (eg, induced by ventilation[41,42]) and the oxidant precursor levels indoor and outdoor.[35] Even though, several models describing indoor air pollution from different sources exist,[34,43-46] none of these addresses both the particle and gas-phase emissions from cooking, where the aforementioned parameters driving the pollutants emission, their transformation, and their losses can be systematically varied.

Practical Implications

- The model can be used for regulating indoor cooking emissions.
- Particle and organic gas emissions indoors are dominated by cooking processes.
- Higher cooking temperatures and frying processes enhance emissions significantly.
- Concentrations may be substantially reduced with a proper ventilation.

Here, we have developed a modeling framework for estimating the influence of cooking processes on the indoor concentration of different compound classes. Pollutant emission rates used as model input parameters are based on a set of more than 100 cooking experiments including vegetable and meat frying and vegetable boiling. These pollutants include primary organic aerosols, acrolein, short-chain saturated carbonyls, long-chain saturated and unsaturated carbonyls, and terpenes. Model input parameters also comprise the reaction rates of these compounds against OH radicals and ozone and their secondary organic aerosol yields determined based on 16 smog chamber experiments. The first part of the paper describes the model implementation and input parameters, while in the second part the impact of residential cooking emissions on indoor and outdoor air is discussed and the main parameters driving the emission concentrations are identified.

2 | METHODS

2.1 | Experimental setup

The emission factor data as well as the specific reaction rates and secondary organic yields for the different compound groups were obtained from three measurement campaigns in 2012, 2014, and 2015. The measurement setup was similar for all three campaigns and is described in detail elsewhere.[18,19] Direct emissions generated during more than 100 cooking experiments were measured. Cooking processes studied include

1. Olive, canola, and sunflower oil heating at different temperatures;
2. Meat shallow frying and charbroiling at different temperatures;
3. Vegetable frying;
4. Deep frying;
5. Vegetable boiling; and
6. Condiment use (herbs and pepper).

The emissions from selected processes were injected into a simulation chamber to study their transformation upon aging. The chamber setup for the 2014 campaign is thoroughly described in Klein et al. (2016b),[19] while in 2012 the setup was similar to that described in Platt et al. (2014,2017).[47,48] After the emissions were injected and well equilibrated

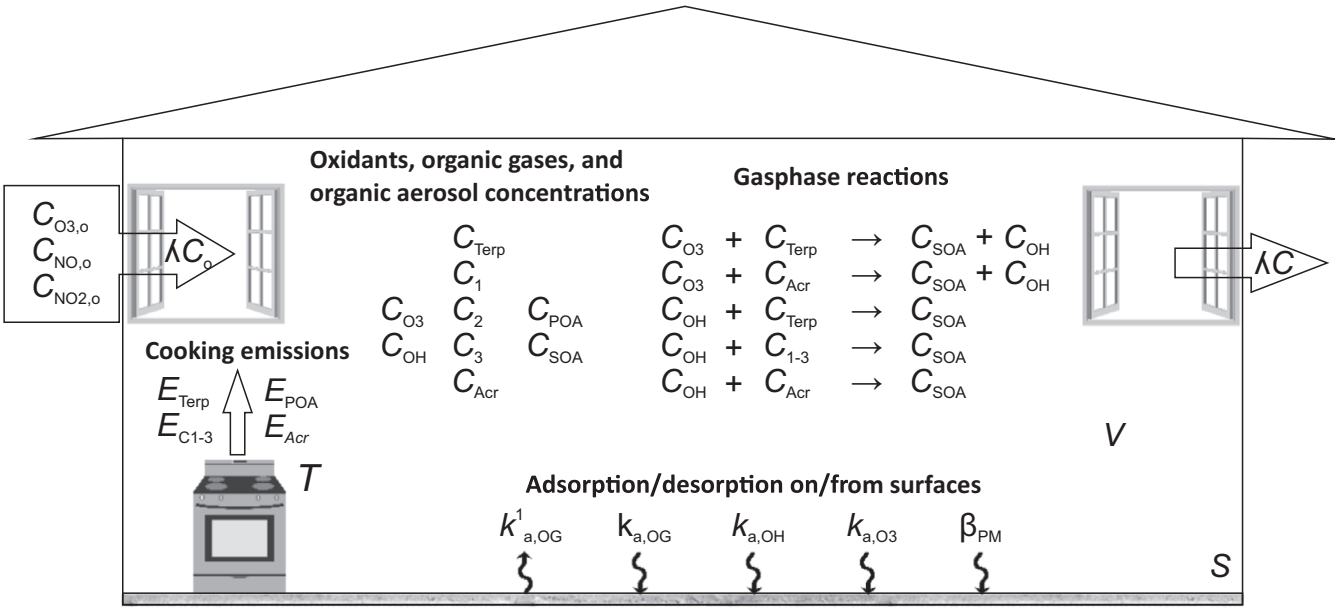

FIGURE 1 Model schematic

in the chamber, 4 sets of 10 UV lights, situated around the chamber, were switched on to induce aging. During 2014 measurements, nitrous acid (HONO), which forms OH radicals via photolysis, was introduced into the chamber at a flow rate of about 2 L min^{-1}. This was not the case during the 2012 campaign, which resulted in significantly lower OH concentrations. The OH exposure in the chamber during both campaigns was estimated by measuring the decay of the d9-butanol,[49] introduced into the chamber through heated lines. All experiments were conducted at 50% relative humidity and a temperature of 20°C.

2.2 | Instrumentation

Non-methane organic gases were measured using a proton-transfer time-of-flight mass spectrometer (PTR-TOF-8000, IONICON Analytik G.m.b.H.) operated in H_3O^+ mode. This limits the measurements to NMOG with a proton affinity higher than that of water. A detailed description of the instrument can be found elsewhere.[50] Operating conditions and data treatment procedures are described in Klein et al. (2016a).[18]

The primary and secondary organic aerosol loads were obtained from a high-resolution time-of-flight aerosol mass spectrometer (HR-TOF-AMS, 600°C vaporizer temperature, Aerodyne Research, Inc.). The instrument was equipped with a PM2.5 lens enabling us to measure particles with a vacuum aerodynamic diameter of up to 3 μm.[51] A detailed description of the instrument and data treatment procedures can be found in DeCarlo et al. (2006).[52]

3 | MODEL FRAMEWORK

The scheme in Figure 1 illustrates the fate of cooking emitted organic gases (OG) and aerosol (POA) in the model and the variables used in the mass balances and secondary organic aerosol (SOA) production expressions. The model used is a box model; that is, the mass balance equations for each pollutant assume the indoor environment to be a single well-mixed volume with air exchange due to infiltration. The OG concentrations in both the indoor air and the indoor surfaces are simulated in the model. The OGs are grouped into five different compound classes according to their chemical nature, reactivity against oxidants, and SOA yields. These classes include

1. C1 compounds, which refer to carbonyls with less than six carbon atom backbone (mainly acetaldehyde, propylaldehyde, butylaldehyde, pentylaldehyde from meat cooking, and acetone from vegetable cooking, see Klein et al. (2016a)[18]);
2. C2 compounds, which refer to saturated carbonyls with more than five carbon atom backbone (see Klein et al. (2016a)[18]);
3. C3 compounds, which refer to unsaturated carbonyls with more than five carbon atom backbone (see Klein et al. (2016a)[18]);
4. ACR which consists only of acrolein (see Klein et al. (2016a)[18]);
5. Terpenes, which comprise p-cymene, monoterpenes, oxygenated monoterpenes, and sesquiterpenes (see Klein et al. (2016a)[18]).

In addition to directly emitted POA, SOA production from the oxidation of terpenes (TerpSOA) and of the aggregate of C2, C3, and ACR (CSOA) is modeled. The sum of both fractions shall be considered as our best estimate of the total indoor SOA (totSOA) from indoor cooking processes.

The model simulates the emissions from meat frying, vegetable frying and boiling, deep frying, condiment use, and oil heating for the three different frying processes considered here. In the following, let *i* and *j* be the indices for a generic compound class emitted from a generic cooking process, respectively. The evolution of the mass concentration (in μg m^{-3}) of a compound *i*, $C_i|_g$ (where g denotes the

gas-phase), with time, *t*, may be described by the following generalized differential Equation 1:

$$\frac{C_i|_g}{dt} = \sum_j \text{Prod}_{i,j} - \text{Loss}_i \quad (1)$$

where $\text{Prod}_{i,j}$ denotes the production rate of a compound *i* from a cooking process *j* and Loss_i the loss rate of *i*. In the Sections 3.1 and 3.2, we present the modeling of the production and loss processes for OGs and POA, respectively. The representation of the SOA production from OG oxidation is described in Section 3.1, and the generation of input model parameters is detailed in Section 3.1. Input variables were modeled as probability distributions and used in a Monte Carlo operation such that distributions of resulting time-dependent concentrations could be predicted and the influence of inputs on these concentrations could be quantified. Later, *k* shall represent a generic Monte Carlo trial.

3.1 | Production rates

The production term in the model is developed to mimic as faithfully as possible the dependence of the emissions to the cooking processes and conditions applied, based on our experimental data. The processes applied to generate these data are in agreement with cooking book recommendations and our experimental data.

The time-dependent production term (in µg m^{-3} s^{-1}) of a primary compound *i* may be presented by Equation 2:

$$Prod_{i,j} = \frac{x_j * \varphi'_j(t) * ER_{i,j}}{V_{house}} \quad (2)$$

The definition and the general formulation of the different parameters in Equation 2 are expressed explicitly in the following:

- V_{house} (in m^3) is the total house volume calculated as the total house floor area (A_{house}) times the room height (h_{room}) (from European commission report [53]). A_{house} is expressed as the product between the house area per person,[54] A_{pers}, and the number of persons per household,[54] N_{pers}. The occurrence of a given number of persons in a given space is a classic Poisson process, where N_{pers}, which occurs independently and with a known average rate, is a discrete independent random variable following a Poisson distribution. In European households, the average N_{pers} is 2.3 persons, leading to the following probabilities: $\mathbb{P}(N_{pers}=0)$, $\mathbb{P}(N_{pers}=1)$, $\mathbb{P}(N_{pers}=2)$, $\mathbb{P}(N_{pers}=3)$, $\mathbb{P}(N_{pers}=4)$ equal to 0.1, 0.23, 0.27, 0.20, and 0.12, respectively. To avoid empty households in the model, we have considered N_{pers} to rather follow a shifted geometric distribution, which yields similar results: $\mathbb{P}(N_{pers}=0)$, $\mathbb{P}(N_{pers}=1)$, $\mathbb{P}(N_{pers}=2)$, $\mathbb{P}(N_{pers}=3)$, $\mathbb{P}(N_{pers}=4)$ equal to 0, 0.43, 0.24, 0.14, and

TABLE 1 Input parameters used in the Monte Carlo simulations for the description of the household, loss rates, and pollutant outdoor concentrations

	GM	GSD	P10	P25	P50	P75	P90
$\mathbf{N_{pers}}$ (#)[a]	–	–	1	1	2	3	4
$\mathbf{A_{pers}}$ (m^2)[a]	45	1.5	27	34	46	60	75
$\mathbf{h_{room}}$ (m)[a]	–	–	2.5	2.6	2.7	2.9	3.1
$\mathbf{V_{house}}$ (m^3)	–	–	91	121	210	397	650
$(\mathbf{S/V})_{\mathbf{house}}$ (m^2 m^{-3})[b]	3.4	1.2	2.7	3	3.4	3.9	4.4
$\boldsymbol{\lambda} \times 10^5$ (s^{-1})[c]	20	2.1	8	12	20	34	52
$\boldsymbol{\beta_{PM}} \times 10^5$ (s^{-1})[c]	22	1.35	15	18	22	27	32
$\boldsymbol{\beta_{O_3}} \times 10^5$ (s^{-1})[d]	70	1.5	40	53	71	91	114
$\boldsymbol{\beta_{NO_2}} \times 10^5$ (s^{-1})[e]	33	1.5	19	25	33	43	55
$\mathbf{J_{HONO}} \times 10^5$ (s^{-1})[f]	5.7	2.48	1.7	3	5.8	10	18
$\mathbf{C_{O_3,out}}$ (ppb)[g]	26	2.01	11	18	27	44	66
$\mathbf{C_{NO,out}}$ (ppb)[g]	1.8	3.53	0.34	0.81	1.8	4.4	9.3
$\mathbf{C_{NO_2,out}}$ (ppb)[g]	–	–	0.84	1.8	4.2	11	23

[a]Data are relative to European households from the European commission report on standard building specifications[53] and Eurostat.[54] N_{pers} is generated using a geometric distribution with an average of 2.3 capita per household (see text for more explanations regarding the choice of the geometric distribution); $h_{room} = h_{min} + h_k$, where h_{min} is the minimum ceiling height for European living spaces = 2.4 m and h_k a random variable following a lognormal distribution with GM = 0.3 and a GSD = 1.8. V_{house} is $N_{pers} \times A_{pers} \times h_{house}$.
[b]Hodgson et al. (2004).[55]
[c]Weisel et al. (2005).[56]
[d]Lee et al. (1999)[57]; Morrison et al. (2011).[58]
[e]Spicer et al. (1993).[59]
[f]Alvarez et al. (2013).[60]
[g]EPA (2013)[61] monitoring data, similar to data in Europe. $C_{NO2,out} = C_{NO,out} \times (NO_2/NO)_{out}$ with $(NO_2/NO)_{out}$ being the ratio between $C_{NO_2,out}$ and $C_{NO,out}$ generated following a lognormal distribution with GM = 2.4 and a GSD = 1.4.

0.08, respectively. A_{pers} follows a geometric distribution with a geometric mean, GM, equal to 45 m^2 [54] and a geometric standard deviation, GSD, equal to 1.5 (calculated based on the intercountry and intracountry variability for A_{pers}). From these calculations, we estimate a median V_{house} of 210 m^3 (probability density function of house sizes can be seen from Figure S1), which is smaller than household volumes in the US,[62] GM = 387 m^3. All the input parameters can be found in Table 1.

- x_j is an independent random variable which takes a value of either 1 or 0, when the process j does or does not occur, respectively. For each Monte Carlo simulation k, x_j is generated through a Bernoulli trial, with a predefined probability of $x_j = 1$, $\mathbb{P}(x_j = 1)$, equal to p_j. As the logarithm transformed outputs are examined in the Result section, we have replaced $x_j = 0$ by $x_j = 10^{-9}$. The value for $x_{\text{oilheatingforj}}$ is set to be equal to x_j, with j = vegetable frying, meat frying, or deep frying (ie, oil heating for a certain frying process only occurs if this process occurs). We have also set $\mathbb{P}(x_{\text{vegetablefrying}} \cup x_{\text{vegetableboiling}})$ and $\mathbb{P}(x_{\text{vegetablefrying}} \cap x_{\text{vegetableboiling}})$ equal to 0.9 and 0.1, respectively. Simulations where $x_j = 0$ for all processes are excluded (no food cooked). For the accepted simulations (in total 1940 out of 2000), meat frying, vegetable frying, vegetable boiling, deep frying, and condiment use occur for 77, 54, 51, 5.3, and 50% of the times, consistent with the p_j values we have set. This approach yields reasonable amounts of food cooked per person (Figure S2, eg, it is highly improbable that all processes occur together and that the amount of food per person exceeds a certain threshold), while still accounting for the variability in the emissions from the different processes applied.
- $\varphi'_j(t)$ is a (unitless) kernel function representing the derivative of the cooking time as a function of time, such that

$$\varphi(t) = \int \varphi'_j(t) \tag{3}$$

and

$$\varphi(\infty) = \int_0^{\infty} \varphi'_j(t) = \Delta t_j \tag{4}$$

Here, Δt_j denotes the total time for a given cooking process j, where Δt_j equals the product of the number of cooking batches, NB_j, times the cooking time per batch, Γ_j. The number of cooking batches is set to one for all processes, except for deep frying where a batch per two persons is considered. $\varphi'_j(t)$ used here takes the form of a product between two sigmoid functions, as written in Equation 5.

$$\varphi'_j(t) = \left\{1 - \frac{1}{1 - \exp\left(\frac{\Delta t_j + t_j - t}{\tau_{\text{fall}}}\right)}\right\} \times \left\{\frac{1}{1 - \exp\left(\frac{t_j - t}{\tau_{\text{rise}}}\right)}\right\} \tag{5}$$

- Here, t_j is the starting time of a cooking process j, with $t_j = 0s$ for oil heating, $t_j = \Delta t_{\text{oilheating}}$ for vegetable, meat, and deep frying (as the frying only occurs after heating the oil) and $t_j = 600s$ for vegetable boiling (time required for bringing water to boil). For condiment use, the same rules as for $\Delta t_{\text{condimentuse}}$ apply to $t_{\text{condimentuse}}$. τ_{rise} = 20 s and τ_{fall} = 8 s are the time constants for the beginning and the end of a cooking process j, respectively. These time constants are chosen based on an average heating rate observed during our experiments. While any other kernel could be used for the representation of the progress of a cooking process, we opted for a continuous function, such that the concentrations of the different components in time can be differentiated. Other kernel forms also tested yielded very similar results. Δt_j values are largely based on our experiments and are consistent with cookbook recommendations.[63] The geometric mean (geometric standard deviation) for $\Delta t_{\text{oilheating}}$, $\Delta t_{\text{meatfrying}}$, $\Delta t_{\text{vegetablefrying}}$, $\Delta t_{\text{vegetableboiling}}$, and $\Delta t_{\text{deepfrying}}$ is set to 240, 900, 1500, 1500, and 600 s (1.2, 1.4, 1.4, 1.4 and 1.2), respectively. The values for $\Delta t_{\text{condimentuse}}$ are set to be equal to either $\Delta t_{\text{meatfrying}}$ or $\Delta t_{\text{vegetablefrying}}$ (with equal probability) if both (meat and vegetable frying) occur. If only one of the two processes occurs, then $\Delta t_{\text{condimentuse}}$ takes the value of Δt_j set for this process. Otherwise, $\Delta t_{\text{condimentuse}}$ is set to zero. Considering that cooking activities occur simultaneously and twice a day yields an estimated time spent on cooking per day of around 1 hour. The distribution of these estimated values is in accordance with the reported number of hours spent for cooking per household per day, ranging from 0.5 hours for households in South Korea to 1.9 hours in India.[64]
- $\text{ER}_{i,j}$ represents the emission rate of a product i from a process j. The expression of the emission rates depends on the cooking process applied. For oil heating where emissions depend on the oil surface per m^2 of oil S_j^{oil}, $\text{ER}_{i,j}$ is

$$\text{ER}_{i,j=\text{oilheating}} = S_j^{\text{oil}} * \text{ER}_{i,j}^{s} \tag{6}$$

Here, $ER_{i,j}^{s}$ (in μg m^{-2} s^{-1}) denotes the emission rate of a product i from a process j per m^2 of oil. The geometric mean for S_j^{oil} was set to 0.020 m^2 for shallow frying (assuming only part of the pan to be covered by oil when pan frying) and 0.045 m^2 for deep frying (GSD = 1.5 and 1.05). Based on our experimental results, $ER_{i,j}^{s}$ follows an Arrhenius behavior and therefore is expressed against the oil temperature T_j^{oil} (in K), as follows:

$$\ln(\text{ER}_{i,j}^{s}) = \ln(A_i^{s}) - \frac{B_i^{s}}{T_j^{\text{oil}}} \tag{7}$$

In Equation 7, A_i^{s} (in μg m^{-2} s^{-1}) and B_i^{s} (in K) are the Arrhenius constants determined from our experimental data, reported for the different species in Table 2. The oil temperatures were assumed to follow a lognormal distribution with GM equal to 165°C and 190°C (GSD = 1.07 and 1.03), for shallow frying and deep frying, respectively, based on the average temperatures applied during our experiments. To account for emission variability, we have generated temperature-dependent $\text{ER}_{i,j}^{s}$ probability distributions using the prediction intervals from the error analysis of the linear regressions of the experimental $\text{ER}_{i,j}^{s}$ data against $(1/T_j^{\text{oil}})$ (Table 2), according to Equation 8:

$$\text{ER}_{i,j}^{s} = \exp\left\{\ln(A_i^{S}) - \frac{B_i^{S}}{T_j^{\text{oil}}} + SE_i^{S} * t_{\text{dist,dF}} * \sqrt{1 + \frac{1}{dF} + \frac{\left(\frac{1}{T_j^{\text{oil}}} - \frac{1}{T_j^{\text{oil}}}\right)^2}{\text{SSD}\left(\frac{1}{T_j^{\text{oil}}}\right)}}\right\} \tag{8}$$

Here, SE_i^S is the regression standard error calculated as the square root of the sum of unexplained variance normalized by the degree of freedom (dF = 26). $t_{dist,dF}$ is the student distribution for dF = 26, and $(1/T_j^{oil})$ and $SSD(1/T_j^{oil})$ are the average temperature inverse and its associated sum of squared deviations, respectively.

For any other cooking process, it is convenient to express $ER_{i,j}$ as a function of the amount of raw food cooked, as data pertinent to purchased goods are typically accessible. Accordingly, $ER_{i,j}$ may be written as

$$ER_{i,j\neq oilheating} = \frac{N_{pers} * \bar{M}_j * ER_{i,j}^M}{p_j * NB_j} \quad (9)$$

where $\bar{M}_j$ (in kg) designates the average raw food mass per person per meal (considering two meals per day) cooked following a process j, and $ER_{i,j}^M$ (in μg kg^{-1} s^{-1}) the emission rate of a product i from j per one kg of food cooked.

For vegetable boiling, deep frying, and condiment use, independent values for $ER_{i,j}^M$ are utilized, as indicated in Table 3. Terpenes are emitted from vegetables and from condiments, while vegetable boiling emits small amount of POA. Meanwhile, large amounts of POA and aldehydes are emitted from deep frying. For vegetable and meat frying, temperature-dependent $ER_{i,j}^M$ probability distributions were generated (here, A_i^M, in $\mu g\,kg^{-1}s^{-1}$, and B_i^M, in K are used), using the parameters in Table 2 and similar equations as Equation 7 and Equation 8. The same temperature, T_j^{oil}, is kept for oil heating and frying. Most of the variance in the relationship between $ER_{i,j}^S$ and T_j^{oil} inverse can be explained by the emission variability with the type of oil used. We note that compared to oil heating only, emission rates manifest a weaker dependence on temperature, especially for species whose emissions are enhanced in the presence of food.[18] These include small aldehydes present in the meat (included in C1), acetone present in onions (included in C1), and POA emitted from the contact between food liquids and hot oil. In addition, the presence of food may change the oil surface properties (eg, total surface, temperature), which in turns varies the emission rates from oil heating.

Ample data on average yearly consumption per capita exist in the literature including reports for different countries and different types of food. These data will be used to determine our best estimate for $\bar{M}_j$ values. Meat consumption data calculated using a

TABLE 2 Arrhenius input parameters determined by fitting the experimental $ER_{i,j}^S$ and $ER_{i,j}^M$ data against the temperature inverse, which can be used for the determination of temperature-dependent emission rate probability distributions used in the Monte Carlo simulations. A_i denotes both A^S and A^M, in μg m^{-2} s^{-1} and μg kg^{-1} s^{-1} for heating oil and for frying processes

	B_i (K)	lnA_i	SE_i
Parameters for $ER_{i,j}^S$			
POA	9183	24.9	0.6
ACR	8461	23.5	0.4
C1	5670	17	0.5
C2	10 352	28.7	0.4
C3	9128	25.7	0.5
Parameters for $ER_{i,j}^M$			
POA	4607	12.4	0.5
ACR	5700	14.5	0.4
C1	2831	9.8	0.3
C2	6114	16.6	0.4
C3	5718	15	0.3

Note: The standard error is calculated as the square root of the sum of unexplained variance normalized by the degree of freedom (dF = 26). Other parameters used include the average of the temperature inverse (0.00228 K^{-1}) and the associated sum of squares of deviations (1.1 × 10^{-6}K^{-1} and 2.0 × 10^{-6} K^{-1}).

TABLE 3 $ER_{i,j}^M$ data for deep frying and vegetable boiling used in the Monte Carlo simulations

	GM	GSD	P10	P25	P50	P75	P90
$ER_{i,deepfrying}^M$ (μg kg^{-1} s^{-1})							
POA	7.6	2.25	2.8	4.3	7.6	14	22
ACR	4.2	1.29	3	3.5	4.2	5	5.8
C1	5.7	1.21	4.5	5.1	5.7	6.5	7.3
C2	17	1.2	13	15	17	19	21
C3	34	1.31	24	29	34	41	47
Terp	–	–	–	–	–	–	–
$ER_{i,vegetableboiling}^M$ (μg kg^{-1} s^{-1})							
POA	0.0085	1.2	0.0067	0.0075	0.0085	0.0096	0.011
ACR	–	–	–	–	–	–	–
C1	1.7	1.2	1.4	1.5	1.7	1.9	2.1
C2	–	–	–	–	–	–	–
C3	–	–	–	–	–	–	–
Terp	0.65	1.21	0.51	0.57	0.64	0.73	0.83

Note: Terp are also emitted from vegetable frying and from condiment use with $ER_{Terp,vegetablefrying}^M = ER_{Terp,vegetableboiling}$ and $ER_{Terp,condimentuse}^M$ = 750 μg kg^{-1} s^{-1}, respectively.

trade balance approach would yield the carcass mass availability, which ranges between 70 and 120 kg per capita per year for developed countries.[65] This estimate does not include losses in retail and food service, and thus does not represent the actual raw meat mass purchased for cooking. Losses in retail are estimated to be 5% for red meat and poultry,[66] and another 5% loss can be estimated as food waste [67] (amount not cooked at all). Losses due to deboning, trimming, and cooking are not considered as our emission rates are normalized to the raw meat mass cooked (were these losses to be considered, the meat mass available per capita would be half of the carcass mass availability, based on USDA [68]). Based on these estimates, we determined a geometric mean value for $\bar{M}_{meatfrying}$ of 0.120 kg per capita per meal. Elmadfa (2009)[69] estimates an average intake of vegetables, starchy roots, and potatoes of about 400 g per capita per day in European countries, similar to estimates for the United States (460 g, PBH foundation[70]). These numbers were used to generate a geometric mean value for $\bar{M}_{vegetablecooking} = 0.2$ kg. Half of the mass of vegetable cooked was considered boiled and the other fried. Geometric mean values for $\bar{M}_{deepfrying}$ and $\bar{M}_{condiments}$ are set to 1.0×10^{-2} kg and 1.2×10^{-3} kg (considering an average yearly consumption of condiments of 900 g, based on ESA[71]), respectively. For all processes, we varied the amounts of food used per capita within 25% (ie, GSD = 1.25). We calculate the total mass of raw food cooked per person, M_{food} in kilogram (Figure S2), as the sum of M_j from all processes, with average M_{food} equal to 0.37 kg.

The production rates from all processes were integrated against time, which provides the total mass of a component *i* emitted per volume. Assuming that cooking occurs twice a day, we estimated the average amount of *i* emitted per time per volume, E_i, which can be directly compared to scaled emission rates of the different compounds reported in the literature (see, eg, Figure 2).

3.2 | Loss rates

The loss term includes (a) transport to outdoor of gas- and particle-phase components due to air exchange, (b) POA and SOA deposition, (c) OG oxidation, and (d) OG sorption onto indoor surfaces.

3.2.1 | Particle losses

The loss of particles (PM, with PM = POA or SOA) can be described as follows:

$$Loss_{PM} = \overbrace{\lambda * C_{PM}}^{\text{exchange}} + \overbrace{\beta_{PM} * C_{PM}}^{\text{deposition}} \quad (10)$$

where λ (in s^{-1}) is the air exchange rate, due to infiltration and or open doors and windows and β_{PM} (in s^{-1}) the particle deposition rate (Table 1). β_{PM} is dependent on particle size, turbulence, and the available surface in a house. These dependences are weak in the range of conditions encountered in indoor environments. First, particles in the accumulation mode (0.1–1 μm), such as those present in cooking emissions, have very similar deposition rates.[72]

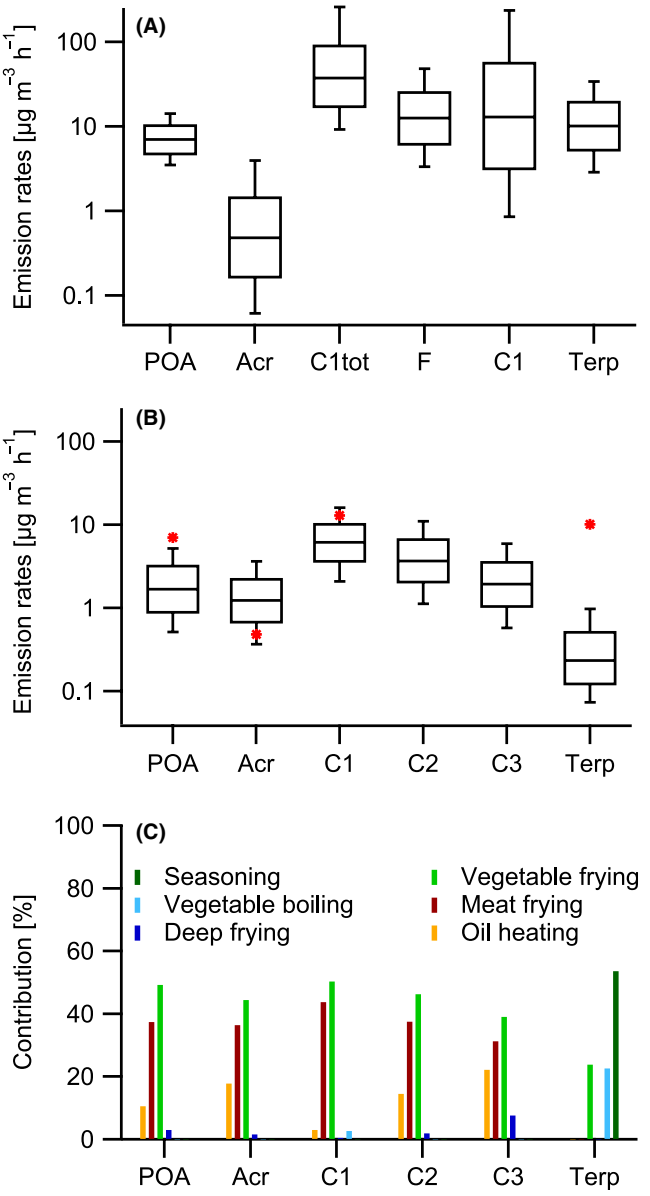

FIGURE 2 Production rates of POA and organic gases from cooking and other indoor sources. Mean values as well as 5th and 95th percentiles (whiskers) and 25th and 75th percentiles (box) are shown for modeled total indoor source emission rates from Waring (2014) [34] (A) and for modeled cooking emission rates from this study (B) as well as the contributions of the different cooking processes to the total emissions (C) of POA, acrolein (Acr), formaldehyde (F), saturated carbonyls with less than 6 carbons (C1tot) or excluding formaldehyde (C1), saturated aldehydes with more than 5 carbons (C2), unsaturated carbonyls with more than 5 carbons (C3), and terpenes (Terp). Red stars in B are median values from A

Second, turbulence, which is typically driven by the temperature profile indoor and air velocity/exchange rate, has little to no influence on the deposition behavior. For example, particle deposition rates have been reported to vary by <20% in the range of air velocity relevant for indoor environments (0-0.5 km h^{-1}, Thatcher et al. (2002)[72]). Third, as the variation of the particle deposition rates is linear with the S/V ratio, this parameter, which varies by

TABLE 4 Lognormal parameters (GM: geometric mean and GSD: geometric standard deviation) for the reaction rates of cooking-related organic gases against hydroxyl radicals and ozone

	GM	GSD	P10	P25	P50	P75	P90
$k_{OH} \times 10^{11}$ (molec^{-1}cm^{3}s^{-1})							
ACR[a]	1.8	1.17	1.5	1.7	1.9	2.1	2.3
C1[c]	1.5	1.19	1.2	1.4	1.5	1.7	1.9
C2[a]	2.2	1.23	1.7	1.9	2.2	2.5	2.8
C3[a]	5	1.19	4	4.4	5	5.6	6.3
Terp[c]	2.9	1.36	2	2.4	2.9	3.6	4.3
$k_{O_3} \times 10^{18}$ (molec^{-1} cm^3 s^{-1})							
ACR[d]	2.6	1	—	—	—	—	—
C1[e]	—	—	—	—	—	—	—
C2[e]	—	—	—	—	—	—	—
C3[f]	6.9	2.61	1.8	3.4	7	13	23
Terp[c]	250	1.54	150	190	250	340	440

[a]From this study based on the decay of these compounds against time and the estimated C_{OH} in the chamber based on the d-9 butanol decay (equivalent to using the relative decay technique).
[b]From Atkinson and Arey (2003).[73] Rates were weighted by the compounds' relative abundances, and these abundances were varied through an initial, separate Monte Carlo simulation to determine the variability of these rates.
[c]Using Terp decay rates and C_{OH} and C_{O_3} from this study and ($k_{OH,Terp}/k_{O_3,Terp}$) ratios for a mix of terpenes from Atkinson and Arey (2003),[73] through a separate Monte Carlo simulation.
[d]From NIST (2016)[74] (taken from Grosjean et al. (1993)[75]).
[e]Considered to be inert against ozone.
[f]Estimated using the reaction of C3 against hydroxyl radicals, $k_{OH,C3}$, from this study and the relationship between $k_{OH,C3}$ and $k_{O_3,C3}$ reported in Colman et al. (2015)[76] for α, β-unsaturated aldehydes: $\ln(k_{O_3,C3}) = 0.16 \sim \ln(k_{OH,C3}) - 7.55$.

<20% (Table 1), is not expected to significantly affect the deposition rates. Therefore, we have opted for using an independent deposition rate coefficient (β_{PM}), which we vary within the range encountered in indoor environments, similar to previous studies.[34]

3.2.2 | OG losses

The loss term for an *OG i* is formulated in Equation 2 and the processes/parameters therein shall be successively described in the following:

$$\text{Loss}_{OG} = \overbrace{\lambda * [OG]}^{\text{exchange}} + \overbrace{k_{OH,OG} * C_{OH} * C_{OG}|_g + k_{O_3,OG} * C_{O_3} * C_{OG}|_g}^{\text{oxidation}} + \overbrace{k_{a,OG} * \left(\frac{S}{V}\right)_{house} * C_{OG}|_g - \frac{k_{a,OG}}{K_{e,OG}} * \left(\frac{S}{V}\right)_{house} * C_{OG}|_s}^{\text{adsorption/desorption}} \quad (11)$$

Oxidation

We considered the oxidation of the organic gases with hydroxyl radicals and ozone. The reaction of nitrate radicals was not included as their impact on the indoor VOC conversion is expected to be one to two orders of magnitudes lower than the impact of hydroxyl radicals and ozone.[35] In Equation 2, C_{OH} and C_{O_3} denote the hydroxyl radicals and ozone concentrations and $k_{OH,i}$ and $k_{O_3,i}$ are the rate constants for their reactions against OG, respectively.

Determination of OGs reaction rates: The distribution of $k_{OH,i}$ and $k_{O_3,i}$ values, presented in Table 4, are determined from our experimental results or taken from literature when not accessible. We consider in the following that saturated and unsaturated carbonyls react only with hydroxyl radicals, while terpenes may react with both ozone and hydroxyl radicals, given their relative reaction rates and C_{OH} and C_{O_3} under our conditions.

For ACR, we estimate based on our chamber results a median $k_{OH,ACR} = 1.9 \times 10^{-11}$ molec^{-1} cm^3 s^{-1}, in perfect agreement with the literature values[74,77] of $k_{OH,ACR} = 2 \times 10^{-11}$molec^{-1} cm^3 s^{-1}. The reaction of ACR toward ozone was taken from Grosjean et al. (1993).[75]

C1 compounds are produced from the oxidation of higher molecular weight species, and thus, their reaction rates toward hydroxyl radicals could not be reliably determined from our chamber data. Instead, $k_{OH,C1}$ values for the entire class of C1 compounds are determined using the rates of individual compounds from Atkinson and Arey (2003),[73] weighted by the compounds' relative abundances in the emissions. The latter are varied through an initial, separate Monte Carlo simulation to take into account emission variability, resulting in a $k_{OH,C1}$ distribution that could be used in the model.

The reaction rates of C2 compounds against hydroxyl radicals are estimated from our chamber data to range between 1.9×10^{-11} and 2.5×10^{-11}molec^{-1} cm^3 s^{-1} (first and third quartiles), comparable to values reported for linear aldehydes (eg, $k_{OH,hexanal} = k_{OH,heptanal} = 3.0 \times 10^{-11}$molec^{-1} cm^{3}s^{-1}, Atkinson and Arey (2003)[73] or $k_{OH,heptanal} = 3.6 \times 10^{-11}$molec^{-1}cm^{3}s^{-1}, Bowman et al. (2003)[78]).

C3 compounds mainly comprise α, β-unsaturated aldehydes with different carbon chain lengths,[18] depending on the type of oil used. The reaction rates of C3 compounds against hydroxyl radicals are estimated from our chamber data to range between 4.9×10^{-11} and 5.6×10^{-11}molec^{-1} cm^3 s^{-1}. Gao et al. (2009)[79] report similar values for C6, C8, and C9 trans-α, β-unsaturated aldehydes, with $k_{OH} = 4 \times 10^{-11}$molec^{-1} cm^3 s^{-1}. α, β-unsaturated aldehydes react with ozone less efficiently than their alkene structural homologues,[75] as ozone reaction with double bonds is an electrophilic addition. Colman et al. (2015)[76] reported a relationship between $k_{O_3,C3}$ and $k_{OH,C3}$, from the study of the degradation of C7–C9 biogenic α, β-unsaturated aldehydes: $\ln(k_{OH,C3}) = 0.16 \ln(k_{OH,C3}) - 7.55$. Here, we used this relationship together with $k_{OH,C3}$ determined from our chamber to predict $k_{O_3,C3}$ values and their distribution: Estimated $k_{O_3,C3}$ values range between 3.4×10^{-18} and 13×10^{-18}molec^{-1}cm^{3}s^{-1} (first and third quartiles). These rates are relatively low compared to other indoor relevant compounds, such as terpenes.

Unlike the other compound classes, terpenes are highly reactive against ozone and therefore under our chamber conditions may react with both ozone and hydroxyl radicals. The reaction rates of identified terpenes[19] against ozone and hydroxyl radicals span almost two orders of magnitude and therefore cannot be directly used in the

model. In contrast, the average lifetimes of terpenes in our chamber are fairly reproducible. Therefore, in order to determine the average $k_{OH,Terp}$ and $k_{O_3,Terp}$ for the terpene mixture in the chamber, we used another separate Monte Carlo simulation to generate a probability density function of the ($k_{OH,Terp}/k_{O_3,Terp}$) ratio, assuming a randomly generated mixture of the most important mono- and sesquiterpenes identified and using reaction rates from Atkinson and Arey (2003).[73] Using this ratio distribution, the calculated lifetime distributions, and the hydroxyl radicals and ozone concentrations in the chamber for these specific experiments (2.5×10^7 and 1.0×10^{12} molec cm^{-3}, respectively, see Klein et al. (2016b)[19]), we determine an average $k_{OH,Terp}$ and $k_{O_3,Terp}$ of 2.9×10^{-11}molec^{-1} cm^3 s^{-1} (32% error) and 2.5×10^{-16}molec^{-1} cm^3 s^{-1} (54% error), respectively.

Determination of indoor oxidant concentrations: The prediction of C_{OH} and C_{O_3} would require a detailed understanding of indoor oxidant sources and sinks, which in turn entails the knowledge of outdoor reactive gases (O_3, NO_x, and OG), their penetration through the building envelope, their potential indoor sources, and their indoor transformation through photolysis, reactions, and deposition. Waring and Wells (2015)[35] developed a Monte Carlo framework for predicting the indoor C_{OH} and C_{O_3}, considering established and newly realized oxidant sources. A brief description of the oxidant framework and the main processes involved will follow.

In the framework of Waring and Wells (2015),[35] outdoor-to-indoor transport is the principal indoor source of ozone, the initiator and the main driver of indoor chemistry, with a penetration coefficient >0.8.[80] In the model, ozone is lost by reacting in the gas-phase with alkenes [73] or by chemical uptake onto building materials via heterogeneous reaction with surface-sorbed alkenes,[81,82] with an average deposition rate β_{O_3} of 7×10^{-4} s^{-1} (Table 1, Spicer et al. (1993)[59]). As a result, indoor ozone concentrations often correlate with outdoor concentrations and are 20%-70% of ambient values.[83] Owing to their short lifetimes, outdoor-to-indoor transport of hydroxyl radicals is not a significant indoor source [84] and therefore is not considered in the model. An important hydroxyl radical source in the model is the aforementioned reactions between ozone and alkenes and the subsequent rearrangement and decomposition of the resulting stabilized Criegee intermediates. These reactions are traditionally considered the almost exclusive drivers of indoor hydroxyl radicals.[85] However, more recently the photolysis of indoor nitrous acid (HONO) formed from combustion or NO_2 hydrolysis on indoor surfaces [60] has been identified as another potentially important hydroxyl radical source indoors and therefore is included in the model. This source is especially important at high indoor actinic light fluxes in the range of 340-405 nm and in the presence of indoor combustion sources.[35] The hydroxyl radicals are lost by reaction with the OGs and NO_2.

In their framework, Waring and Wells (2015)[35] considered a scenario with stable indoor background concentrations of 91 OGs (from Logue et al. (2011)[86]), variable outdoor O_3 ($C_{O_3,out}$) and NO_x ($C_{NO,out}$ and $C_{NO_2,out}$) concentrations, and variable indoor D-limonene concentrations (C_{lim}). This scenario will be considered here, while other scenarios were tested but provided similar results. By examining the effect of different model inputs on modeled indoor oxidant concentrations, Waring and Wells (2015)[35] determined the most influential parameters and a relationship relating these parameters (VAR_I) with the natural log-transformed outcome variables, $\ln(C_{OH})$ and $\ln(C_{O_3})$:

$$\ln(C_{OH}) = \sum_I RC_{OH,I} * \ln(VAR_I) + y_{int,OH} \quad (12)$$

$$\ln(C_{O_3}) = \sum_I RC_{O_3,I} * \ln(VAR_I) + y_{int},O_3 \quad (13)$$

Here, $y_{int,OH}$ and y_{int,O_3} and $RC_{OH,I}$ and $RC_{O_3,I}$ are the regression intercepts and coefficients for the different input variables taken from Waring and Wells (2015),[35] for both OH and O_3, respectively. Input variables, VAR_I, include $C_{O_3,out}$, $C_{NO,out}$, $C_{NO_2,out}$, C_{lim}, λ, β_{O_3}, β_{NO_2}, and J_{HONO}, where β_{NO_2} is the deposition rate of NO_2 and J_{HONO} the photolysis rate of HONO. We have considered the same distributions for VAR_I as in Waring and Wells (2015)[35]; these are reported in Table 1. While, similar to D-limonene, cooking emitted organic gas reaction with ozone may lead to a decrease (increase) in ozone (hydroxyl radical) concentration, this effect is not significant (<5%) and therefore not considered in the following. This effect has been assessed by adding to C_{lim} in Equations 12 and 13, and the sum of $C_{OG,i}$ scaled by $k_{O_3,i}$ relative to $k_{O_3,lim}$, assuming an OH molar yield for OG_i ozonolysis of 0.86, equals to that of D-limonene ozonolysis.[85]

Sorption

Modeling the sorption of gases onto indoor surfaces is not straightforward. These processes heavily depend on the chemical nature and physical properties of both binding gases and adsorbing material (eg, inhomogeneity, roughness, and composition) and may involve the diffusion of the gases within the material and complex interactions and competition between these gases.[87,88] Here, we did not attempt to reproduce exactly the equilibrium of the gases at the interface through a full-scale, computationally intensive model, while lacking observational constraints for model parameters (measurements in indoor environment where all processes except gas-surface interactions are characterized). Instead, we have opted for a rather simplified approach, where model inputs that represent the surfaces' sorption properties can be effectively varied, such that the sensitivity of the model outputs on the assumed parameters can be assessed. The approach is a linear absorption-desorption model, which assumes the sorption of OGs onto building materials to follow a Langmuir process. The parameters driving the partitioning of a compound between the gas and the absorbed phase are represented in Equation 14. These include (a) the gas adsorption rate, $k_{a,i}$ (in mh^{-1}), (b) the equilibrium partitioning constant, $K_{e,i}$ (in m), and (c) the indoor surface to volume ratio including furniture, $(S/V)_{house}$ (in m^{-1}). The OG_i concentration change due to adsorption is represented by $k_{a,i} * (S/V)_{house} * C_i|_g$, while the change due to desorption is represented by $(k_{a,i}/K_{e,i})*(S/V)_{house}*C_i|_S$, where $C_i|_S$ denotes the surface-sorbed concentration of OG_i expressed as:

TABLE 5 Lognormal distributions of the vapor pressures (Pa) of cooking-related organic gases used in the Monte Carlo simulations

	GM	GSD	P10	P25	P50	P75	P90
ACR	33 331	133	–	–	–	–	–
C1	63 995	173	45 329	54 662	63 995	77 327	90 659
C2	227	187	147	187	227	280	360
C3	53	200	32	41	53	71	89
Terp	133	187	87	108	133	173	200

Note: Data are from Lide et al. (1947),[89] and ranges are determined based on the chemical speciation analysis of the different compound classes determined by the PTR-TOF-MS.

$$\frac{dC_i|_S}{dt} = k_{a,i} * C_i|_g - \frac{k_{a,i}}{K_{e,i}} * C_i|_S \quad (14)$$

Here, we considered two main assumptions. (1) We consider the adsorption of gases on clean surfaces, which is a reasonable assumption if cooking emissions dominate the indoor concentration of the compound of interest. As it shall appear in the following, this assumption may hold for the different carbonyl species, but not for terpenes whose emissions are dominated by detergent use. (2) Based on the Langmuir theory, the adsorption onto a surface depends on the number of available sites, which means that compounds from cooking or other processes will compete for these sites. Nevertheless, under indoor conditions (high $(S/V)_{house}$ and $K_{e,i}$, and low $C_i|_g$), the availability of these sites is not a limiting factor, and therefore, competition between the gases will not be taken into account. Based on assumptions (1) and (2), losses due to adsorption should be considered as highest estimates. The surface of indoor material available per volume is an important parameter for gas-phase adsorption. The $(S/V)_{\text{house}}$ distribution (GM = 3.4, GSD = 1.2) is derived from values reported for 12 houses in California by Hodgson et al. (2004)[55] and is consistent with values for furnished houses reported elsewhere (3.1 m^2 m^{-3}, Thatcher et al. (2002)[72] and references therein). The equilibrium constant, $K_{e,i}$, depends on both the compounds chemical properties and its affinity toward the surface. The study of these data reveals the strong dependence of $\ln(K_{e,i})$ on two parameters:

1. The compound log-transformed vapor pressure, $\log(P_{vap,i})$ which for a given surface $\log(K_{e,i})$ increases with the decrease of $\log(P_{vap,i})$;
2. The type of surface considered where the variation of $\log(K_{e,i})$ for two compounds with given $\log(P_{vap,i})$ with the surface type exhibits an excellent correlation.

By contrast, the gas adsorption rates, $k_{a,i}$, depend on the compound collision frequency and its accommodation coefficient (effective surface), which is intrinsically a function of the surface properties. Literature data support this, showing a very strong effect of the surface considered on $\log(k_{a,i})$ and only a little dependence on the $\log(P_{vap,i})$. We note that the latter might be a mathematical artifact as $\log(K_{e,i})$ and $\log(k_{a,i})$ are obtained simultaneously from fitting experimental data, which may lead to their interdependence.

These complex (real and unreal) interdependences may be effectively taken into account by considering the ensemble of $\log(K_{e,i})$ and $\log(k_{a,i})$ of the different compounds as a single vector, $\vec{v}$ (with ten elements), whose distribution follows a multivariate normal distribution, generated using Equation 15.

$$f(\vec{v}) = \frac{|\sum_{\vec{v}}|^{-0.5}}{2\pi} \exp\left(-0.5(\vec{v}-\mu_{\vec{v}})^T * \sum_{\vec{v}}^{-1} (\vec{v}-\mu_{\vec{v}})\right) \quad (15)$$

Here, $\mu_{\vec{v}}$ is the mean vector containing mean values of $\log(K_{e,i})$ and $\log(k_{a,i})$ for the different OGs and $\sum_{\vec{v}}$ is the variance/covariance matrix presented in Table S1 in the supplement. The mean values for $\log(K_{e,i})$ and $\log(k_{a,i})$ for different compounds are based on their $\log(P_{vap,i})$—see Table 5 and the relationship between average adsorption parameters against $\log(P_{vap,i})$ derived from values reported in An et al. (1999).[90] These average parameters are as follows: $\exp \cdot \vec{v} =$ (0.028, 0.017, 1.2, 3.5, 1.8) and $\exp \cdot \vec{v} =$ (3.1×10^{-5}, 2.7×10^{-5}, 7.8×10^{-5}, 1.0×10^{-4}, 8.6×10^{-5}), which corresponds to $K_{e,ACR}$, $K_{e,C1}$, $K_{e,C2}$, $K_{e,C3}$, and $K_{e,Terp}$ and $k_{a,ACR}$, $k_{a,C1}$, $k_{a,C2}$, $k_{a,C3}$, and $k_{a,Terp}$, respectively.

Based on the K_e values, it can be clearly observed that compounds like long-chain aldehydes and terpenes would tend to stay in the adsorbed phase, while short-chain aldehydes are mostly in the gas-phase. This is consistent with measurements in different indoor environments for a range of organic gases with a similar volatility as the cooking emissions investigated here. For example, Singer et al. (2004)[91] and (2017)[92] reported K_e values between 1 and 3 m and between 2 and 7 m for monoterpenes and for n-alkanes with a carbon number similar to C3 compounds, respectively. The adsorption rates (times the S/V ratio) of gaseous cooking emissions range between 0.4 and 1.2 h^{-1}, comparable to those reported for other compounds (eg, ozone; Table 2) or determined for organic gases from measurements in simulated indoor residential environments (eg, Singer et al. (2004)[91] and (2007)[93]).

The variance of $\log(K_{e,i})$ and $\log(k_{a,i})$ is calculated by propagating the variation of these parameters with the surface properties and their variation due to the change in their composition and therefore their $\log(P_{vap,i})$. We note that $K_{e,i}$ values vary by a factor of 2.6, while $k_{a,i}$ values vary by a factor of 1.7. The covariance between the parameters takes into account their similar dependence on the surface properties (ie, if surfaces in a house are highly adsorptive, then all gases would tend to be sorbed) and the interdependence between $\log(K_{e,i})$ and $\log(k_{a,i})$. The covariance values indicate that the dependence on the surface properties explains

about 90% and 98% of the variability in $\log(K_{e,i})$ and $\log(k_{a,i})$, respectively, while correlation coefficients (R^2) between $\log(K_{e,i})$ and $\log(k_{a,i})$ are around 0.18.

4 | SOA PRODUCTION

SOA production and loss can be described by the following expression:

$$\frac{dC_{SOA,i}}{dt} = y_{SOA,i} * \left(k_{OH,i} * C_{OH} * C_i|_g + k_{O_3,i} * C_{O_3} * C_i|_g\right) - \lambda * C_{SOA,i} - \beta_{PM} * C_{SOA,i} \quad (16)$$

Here, $y_{SOA,i}$ is the SOA yield from the oxidation of a compound *i*. We recognize that SOA yields depend on the activity of the oxidation products in the particle and gas-phase. However, this dependence is minor compared to other effects (eg, oxidation, emission composition, and strength), especially within the range of concentrations encountered in our chamber and indoor. Therefore, this dependence could not be observed within our uncertainties and will not be considered in the model. Further, we note that yields depend on NO_x concentrations, which were typical of ambient atmospheres (10-20 ppb); therefore, we expect the yields determined in our chamber to be representative. From our chamber experiments, we determine an effective yield from the aggregate sum of ACR, C2, and C3 of 0.22, comparable to values reported for the oxidation of alkane compounds with a similar carbon number,[94] while slightly lower values are reported for long-chain saturated carbonyls (0.1-0.2).[95] We determine a higher effective yield for terpenes (42%),[19] expected from the oxidation of a mix of mono- and sesquiterpenes. Single yield values, $y_{SOA,ACR+C1+C2} = 0.22$ and $y_{SOA,Terp} = 0.42$ will be used to model SOA production from carbonyls and terpenes.

5 | RESULTS AND DISCUSSION

5.1 | Emission and loss rates

5.1.1 | Cooking contribution to indoor emissions

Modeled rates of indoor cooking emissions presented in Figure 2 are estimated in μg m^{-3} h^{-1} based on total daily emissions in the entire house assuming two meals cooked per day. Rates are highly variable due to the different cooking processes involved (Figure 2B) and the amount of food cooked (Figure S2), but remain constrained within a factor of <10 (P90/P10) for all species. We compare the emission rates estimated here with those available in the literature from cooking emission studies. To estimate the importance of cooking compared to other indoor emission processes, we also compare these cooking emission rates to those compiled by Warring et al. (2014)[34] representing the sum of indoor emission sources (Figure 2A).

POA emissions (GM rate 1.7 in μg m^{-3} h^{-1}) are dominated by frying vegetables (49%) and meat (37%). Average POA emission factors from frying correspond to 5 mg kg^{-1}, consistent with the range found in previous studies for frying emissions.[96] For example, Schauer et al. (2002)[37] reported the organic aerosol emission factors from vegetable stir frying and potato deep frying to range between 7 and 16 mg kg^{-1}. We note that Asian-style cooking could generate much higher particulate emissions than Western-style cooking (100 mg kg^{-1})[12]; therefore, our results cannot be generalized to other locations. We also note that we have not observed particle emissions from heated empty pans due to desorption/nucleation of sorbed organics recently suggested as a primary source of particles from cooking processes.[39] Therefore, we have not considered this additional source in our model, although such processes can still occur if pans are not cleaned well. Based on the calculations of Waring et al. (2014),[34] we can infer that cooking can explain about half of the total POA emission rates indoor, including smoking.

The general picture is the same for aldehydes but with higher influence from oil heating. Acrolein GM emission rate is estimated as 0.8 μg m^{-3} h^{-1}. While cooking emission rates for acrolein are higher than those estimated for overall indoor sources, they compare well to values from a study estimating cooking-related acrolein emission rates (0.9-1.5 μg m^{-3} h^{-1}) by comparing the acrolein concentrations in a house with and without cooking events.[97] C1 carbonyl emission rates are estimated to be 7.3 μg m^{-3} h^{-1}, mostly generated through frying processes (vegetables: 50%, meat: 43%). Cooking can explain the average emission rates of small carbonyl indoor (neglecting formaldehyde which was not measured in our case), but the maximum values reported by Waring and coworkers are much higher. The emission rates of C2 and C3 carbonyls are estimated as 2.5 μg m^{-3} h^{-1} and 1.3 μg m^{-3} h^{-1}, respectively. This corresponds to a GM emission factor for C2 compounds of 7.5 mg kg^{-1}, a factor of 5 lower than values reported by Schauer et al. (2002)[37] for stir frying of vegetables, potentially due to the different cooking style applied (cooking on a restaurant hot plate). Unfortunately, for most of the C2 or C3 carbonyls, Waring and coworkers did not calculate emission rates. However, the emission rate they reported for hexanal compares well with our estimated GM emission rate, suggesting that large saturated and unsaturated carbonyl indoors may also be dominated by cooking events. Terpenes are generated by frying and boiling vegetables (46%), and the use of seasonings (54%). A recent study reported monoterpene emission rates from several peppers used in Chinese cuisine to range between 2 and 25 μg g^{-1} min^{-1},[20] comparable to the emission rates determined here (45 μg g^{-1} min^{-1} of terpenes half of which are monoterpenes). The emission rates reported for terpenes from all indoor emissions dominated by cleaning product use are about a factor of ten higher than the terpene emission rates calculated for cooking. Therefore, the emission of terpenes from cooking is overall minor compared to other indoor sources, but may play a role in confined kitchens (see below).

5.1.2 | Indoor cooking contribution to outdoor emissions

The analysis above highlights that cooking dominates the emissions of most of the pollutants indoor. Here, we assess the influence of indoor cooking on outdoor air pollution. The origin of cooking organic

aerosol (COA) identified during meal times in ambient air by AMS analysis has been lately challenged and the processes by which this fraction is emitted in the atmosphere remain unclear.[14] The attempt of modeling cooking organic aerosols in Paris [98] and London [99] suggests that the observed concentrations are consistent with an emission rate of 80 and 320 mg person^{-1} day^{-1}, respectively. These rates are significantly higher than the rates determined for indoor cooking, equal to 4.4 mg person^{-1} day^{-1} on average. Indeed, recent results indicate that cooking organic aerosol can be overestimated in ambient air compared to emission measurements by up to a factor of 4 due to the higher relative ionization efficiency (RIE) for this fraction and the use of a collection efficiency (CE) of 0.5.[100] In our case, the CE/RIE factor was constrained based on scanning mobility particle sizer (SMPS) volume measurements using a density of 0.8 consistent with oil droplets obtained by comparing the aerodynamic diameter (from AMS) with the mobility diameter (SMPS). Data are consistent with a CE of ~1, if we assume the default RIE value used for organic aerosols. Despite this possible overestimation of outdoor COA, indoor cooking emissions cannot explain the observed concentration in ambient air, pointing toward the presence of other emission processes. The most likely source of outdoor COA must be related to restaurants, where emission rates are much higher than domestic emissions. For example, emission rates from meat charbroiling are around 15 g kg^{-1},[36] three orders of magnitudes greater than those obtained here or reported for domestic cooking. The significantly higher emissions from commercial kitchens compared to domestic kitchens are also observed in the case of China,[12] where COA is a prominent fraction of the aerosol in urban environments.[101] This hypothesis is consistent with the observation of COA downwind of restaurants [102] and during mobile measurements in restaurant areas.[103] As emissions from restaurants are about two orders of magnitude higher than top-down estimates of cooking emission rates based on ambient measurements, it only requires <1% of food cooked in commercial kitchens to reproduce the observed ambient COA. Therefore, restaurant emissions may be considered as super-polluters. We note that the VOC/COA ratio from these emissions is relatively low (\~1, see Schauer et al. (1999)[36]) compared to that found in domestic cooking emissions (\~10, this study or Schauer et al. (2002)[37]). Therefore, unlike for domestic cooking emissions where SOA production potential may exceed the emitted POA, for commercial cooking this would be unlikely. More studies are necessary to assess the SOA production potential of commercial kitchen emissions.

5.1.3 | Loss rates

In this section, we examine the relative importance of the main processes by which the different pollutants are lost. We compare the integrated losses over 12 hours and note that some processes such as the interaction of the gases with indoor surfaces become a source of VOCs after several hours of emissions. POA is lost equally by exchange and deposition. Meanwhile, acrolein and short-chain carbonyls (C1) are lost almost exclusively through air exchange, as their reaction toward ozone and their deposition onto indoor surfaces are negligible. The losses of the other compounds, that is, C2, C3, and Terp, by different processes are compared in Figure 3. Air exchange remains the dominant process by which all of these gases are lost (median contribution of 80%, 60%, and 56% for C2, C3, and Terp, respectively). Losses by deposition are significant, especially for unsaturated aldehydes with the lowest vapor pressures (median contribution of 34%). Our results are consistent with measurements in different indoor environments reporting that sorption does not greatly affect indoor concentrations of highly volatile species, while it appears to be a relevant indoor process for lower volatility compounds sorbed at rates close to typical residential air change rates (Singer et al. (2004)[91] and (2007)[93]). Oxidation affects predominantly species reactive against ozone, as OH concentrations are very low.

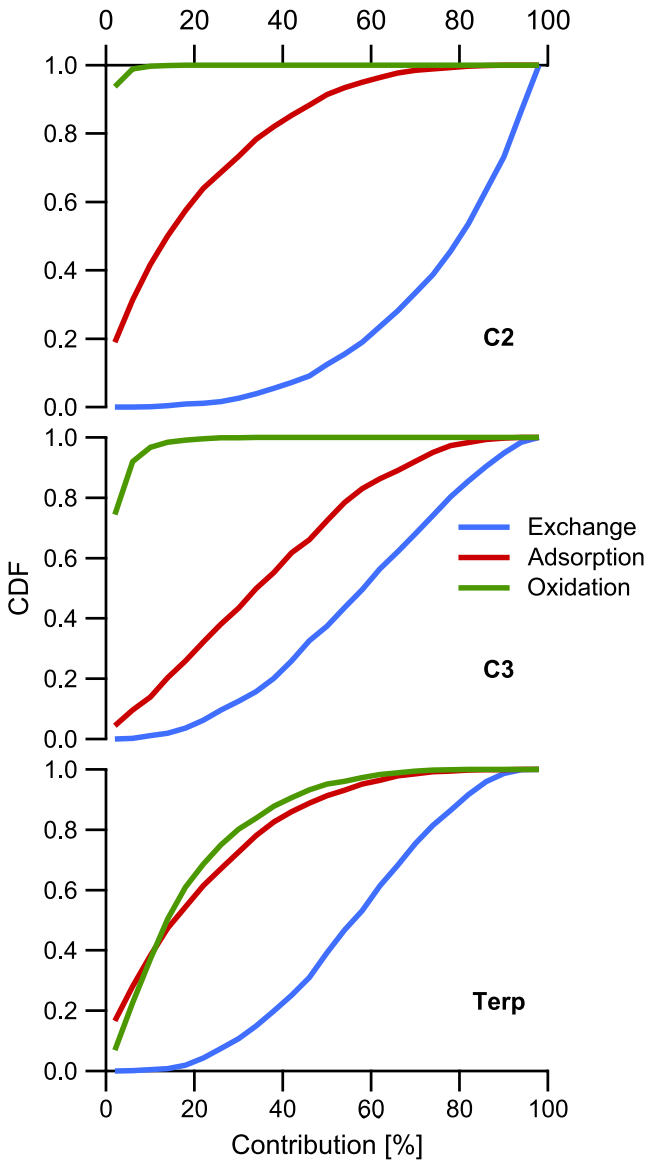

FIGURE 3 Contribution of air exchange, adsorption on surfaces, and gas-phase oxidation to the loss of C2, C3, and terpene compounds during the first 12 hours after being emitted. CDF is the cumulative distribution function which gives the probability that the contribution of a loss mechanism is less or equal than a certain contribution

Accordingly, oxidation is only an effective loss mechanism for terpenes (median contribution of 14%). We note that we have not considered multiphase oxidation processes occurring at indoor surfaces, because of the dearth of quantitative data describing the loss rates of cooking emissions from surfaces. For compounds that are almost quantitatively adsorbed onto surfaces (eg, terpenoids[104]), multiphase oxidation with ozone rivals the homogeneous oxidation in the gas-phase. Therefore, multiphase chemistry is a non-negligible loss mechanism only for terpenes from cooking, which are reactive toward ozone and partition equally between the gas-phase and indoor surfaces. We also note that multiphase chemistry may contribute to the transformation of the unsaturated acids and glycerides contained in the POA deposited onto indoor surfaces, which may constitute a secondary source of carbonyls. However, we note that this source is negligible compared to direct carbonyl emissions from frying (as (C1+C2+C3)/POA ~10 in the emissions). More effort should be devoted in the future to quantify the fate of cooking emissions indoor, with a particular focus on surface deposition and reactions.

5.2 | Indoor pollutant concentrations

The emissions from cooking processes can generate significant gaseous and particulate pollutant concentrations in indoor environments (Figure 4). All gaseous compounds reach their peak concentration about half an hour after the start of the cooking process. The maximum peak concentrations modeled are about 5-600 μg m^{-3} for the C1 compounds (Figure 4B), while the minimum peak concentrations modeled are about 0.5-10 μg m^{-3} for the terpenes (Figure 4E). The peak concentrations for acrolein, C2, and C3 are 2-100 μg m^{-3}, 8-200 μg m^{-3}, and 5-90 μg m^{-3}, respectively (Figure 4A,C,D). This indicates that cooking processes can generate total gaseous pollutant concentrations of up to 1000 μg m^{-3}, spread over the whole house.

The peak concentrations determined from this study compare well with aldehyde concentrations measured in a room directly after different deep frying processes.[105] The average acrolein, C1, C2, and C3 concentrations resulting from the different deep frying processes are 47, 144, 71, and 41 μg m^{-3}, respectively. While acrolein and C1 concentrations decrease constantly to background levels, the concentrations of C2, C3, and terpenes reach a plateau at about 2, 1, and 0.1 μg m^{-3}, respectively. These plateaus are generated by desorption of the compounds from surfaces where they have been deposited before. This nicely explains the long-term odorous contamination of the house after certain cooking procedures like cooking fish or preparing dishes with onions.

The POA reaches its peak concentration after half an hour with 5-200 μg m^{-3} (Figure 4F) followed by a constant decrease to zero within 6 hours. This modeled lifetime of cooking POA is confirmed by measurements of cooking aerosol in a kitchen performed by Hussein et al. (2006)[106] who reported a lifetime of 4-6 hours. The decrease can be explained by irreversible deposition of the particles on surfaces and removal by air exchange. The modeled POA concentrations compare well with measured cooking-related indoor concentrations from various studies conducted by Levy et al. (2002)[107] (200 μg m^{-3}), See and Balasubramanian (2006; 2008)[108,109] (66-190 μg m^{-3}) or Buonanno et al. (2009)[110] (13-389 μg m^{-3}). SOA concentrations reach a maximum after about one hour with 0.05-2 μg m^{-3} (Figure 4J). The maximum amount of SOA formed from the oxidation of the carbonyls

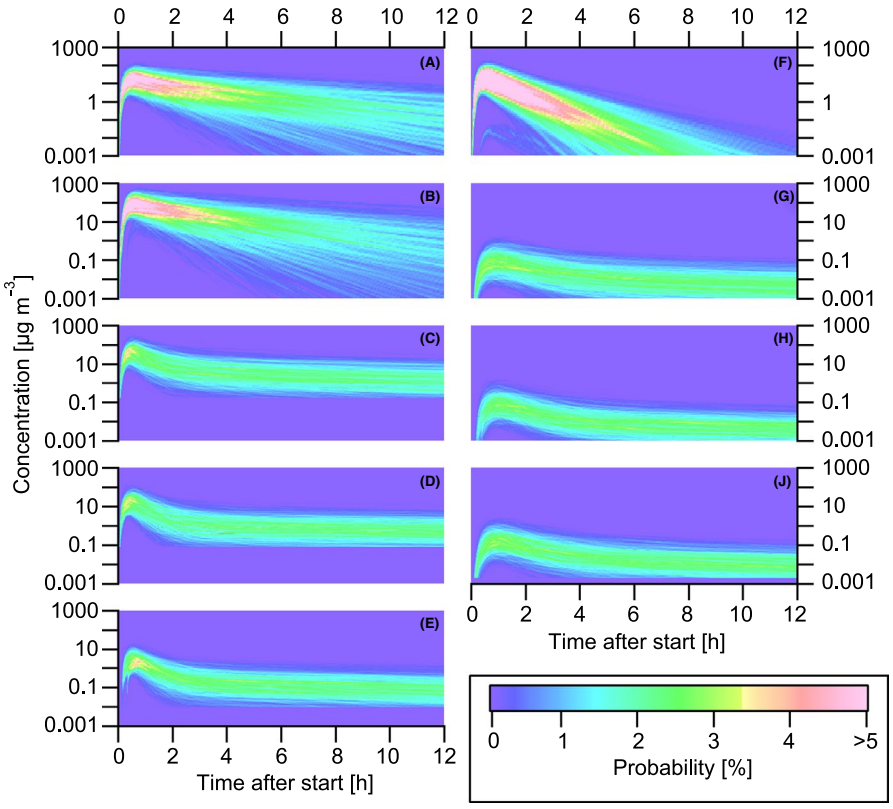

FIGURE 4 Time-dependent probability density functions of indoor pollutant concentrations in European homes originating from Occidental style cooking processes. The left-hand panels show the evolution of the gaseous pollutants, acrolein (A), saturated carbonyls with less than six carbons (B), saturated carbonyls with more than 5 carbons (C), unsaturated carbonyls with more than 5 carbons (D), and terpenes (E). The right-hand panels show the evolution of the particulate species, POA (F), SOA formed from carbonyl oxidation (G), SOA formed from terpene oxidation (H), and total SOA formed (J)

and terpenes (Figure 4G,H) is comparable, with 0.03-1 μg m^{-3} and 0.02-1 μg m^{-3}, respectively. The total SOA decreases slowly, reaching a plateau of about 0.01 μg m^{-3} after 6 h. This plateau is generated by the oxidation of gases which desorb from the surface they have been adsorbed on before. For the first 6 hours after cooking, POA is clearly dominating the indoor particulate concentrations while SOA formation creates a small but constant particle background. The 12-hour average and maximum concentration distributions reveal that frying processes dominate the emissions of most gas- and particle-phase species (Figure 5). As can be seen from the color code, the probability for higher concentrations of acrolein, C1, C2, C3, and POA increase almost monotonically with temperature. As expected, the use of seasonings increases the probability for higher terpene concentrations and SOA formed from terpenes compared to only frying processes. Since the carbonyl emissions are mostly dominated by frying processes, also the formation of SOA from the carbonyls is mainly explained by frying. About half of the SOA formation probability is explained by CSOA and the other half by TerpSOA. The peak of the 12-hour average acrolein probability density function lies around 1-10 μg m^{-3}. This compares well with measurements from residential homes in Canada [111] or California [97] reporting acrolein concentrations of 1 and 6 μg m^{-3}, respectively. Huang et al. (2011)[112] report 17 μg m^{-3} of acrolein in a kitchen after cooking which compares well with our range when the concentration is normalized to the overall house. This indicates that cooking processes are the main source of acrolein in indoor environments generating high enough concentrations to possibly induce negative effects on human health.[113] The C1 distribution peak lies around concentrations of 15 μg m^{-3}; thus, cooking can only explain about one-third to half of the concentrations of small carbonyls measured in residential houses in Europe [114] (45 μg m^{-3}) and the United States [115] (28 μg m^{-3}). Furthermore, cooking can explain with concentrations of 1-10 μg m^{-3} more than half of the average measured concentration of larger saturated aldehydes in Finnish [114] or German [116] homes (9 μg m^{-3} and 16.8 μg m^{-3}). The indoor terpene concentrations of 0.1-1 μg m^{-3} generated from cooking processes are negligible compared to average concentrations measured in indoor environments in Finland [117] and Germany [116] (23 μg m^{-3} and 25.7 μg m^{-3}).

On the other hand, maximum concentrations of terpenes in a kitchen (estimated to be 20% of the total house volume) without much air exchange with the rest of the house can reach up to 50 μg m^{-3}. This compares well with the value reported in our previous study about indoor terpene emissions from cooking processes.[19] Overall, our study shows that cooking is the most important source of gas-phase and particle species indoor having potential deleterious effects on human health highlighting the need for efficient mechanical ventilation in kitchens. The model can be used on the one hand to predict the effect of changes in household settings (eg, hood installation), cooking habits (eg, decrease in frying), and environmental factors (eg, change in the outdoor oxidant levels) on the impact of cooking emissions on indoor air quality. On the other hand, the methodology developed here can be extended to other studies

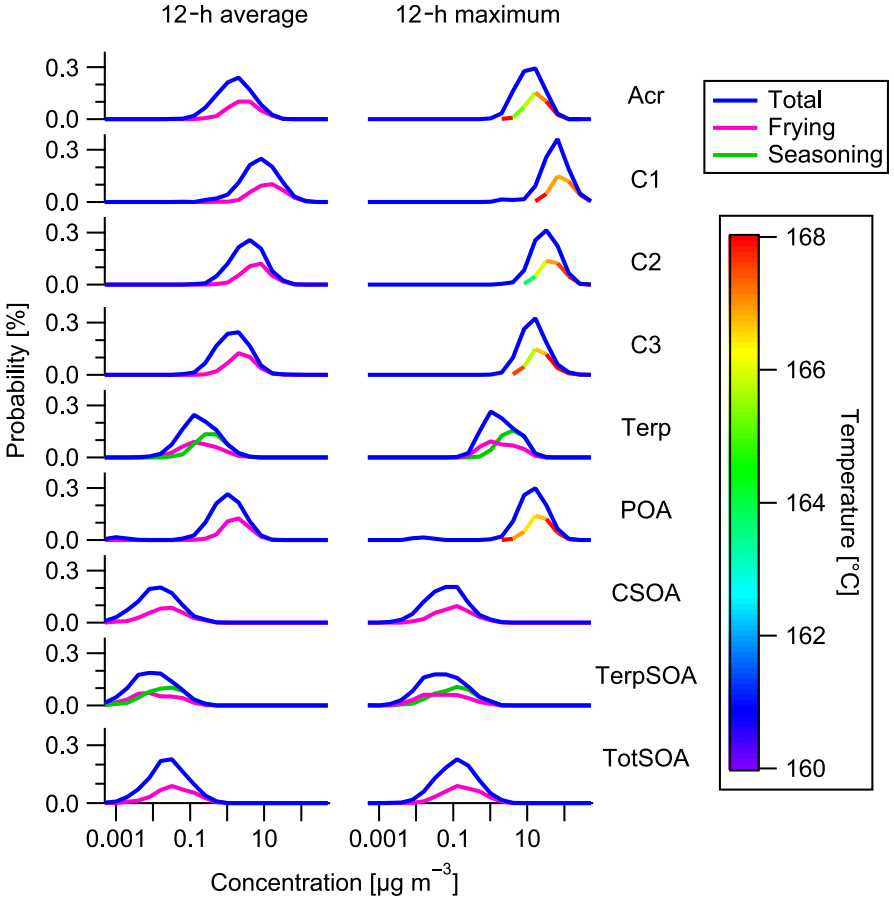

FIGURE 5 Probability density functions of 12-h average and maximum indoor pollutant concentrations in European homes originating from frying processes, the use of seasoning, and the total of all cooking processes. The frying is color coded by the average cooking temperature if relevant for the compound emissions. The left-hand panels show the 12-h averages, and the right-hand panels show the maximum concentration of acrolein (Acr), saturated carbonyls with less than six carbons (C1), saturated carbonyls with more than five carbons (C2), unsaturated carbonyls with more than five carbons (C3), terpenes (Terp), primary organic aerosol (POA), SOA formed from carbonyl oxidation (CSOA), SOA formed from terpene oxidation (TerpSOA), and total SOA formed (TotSOA)

focused, for example, on assessing the impact of cooking (or other emissions) on indoor air quality in developing countries, where cooking habits and household settings are significantly different.

ACKNOWLEDGEMENT

This work was supported by the Swiss National Science Foundation (SNF) within the project AEROCOOK. We acknowledge Nicolas Marchand from Aix Marseille Univ, CNRS, LCE, Marseille, 13331, France, for providing parts of the particle data used for the modeling.

ORCID

Felix Klein https://orcid.org/0000-0002-3680-4735

REFERENCES

1. Brasche S, Bischof W. Daily time spent indoors in german homes — baseline data for the assessment of indoor exposure of german occupants. *Int J Hyg Environ Health*. 2005;208:247-253.
2. Cometto-Muñiz JE, Abraham MH. Compilation and analysis of types and concentrations of airborne chemicals measured in various indoor and outdoor human environments. *Chemosphere*. 2015;127:70-86.
3. Sarigiannis DA, Karakitsios SP, Gotti A, Liakos IL, Katsoyiannis A. Exposure to major volatile organic compounds and carbonyls in European indoor environments and associated health risk. *Environ Int*. 2011;37:743-765.
4. Nasir ZA, Colbeck I. Particulate pollution in different housing types in a UK suburban location. *Sci Tot Environ*. 2013;445–446:165-176.
5. Macneill M, Kearney J, Wallace L, et al. Quantifying the contribution of ambient and indoor-generated fine particles to indoor air in residential environments. *Indoor Air*. 2014;24:362-375.
6. Bhangar S, Mullen N, Hering S, Kreisberg N, Nazaroff W. Ultrafine particle concentrations and exposures in seven residences in northern california. *Indoor Air*. 2011;21:132-144.
7. Wallace L. Indoor sources of ultrafine and accumulation mode particles: size distributions, size-resolved concentrations, and source strengths. *Aerosol Sci Technol*. 2006;40:348-360.
8. Nolte CG, Schauer JJ, Cass GR, Simoneit BR. Highly polar organic compounds present in meat smoke. *Environ Sci Tech*. 1999;33:3313-3316.
9. Wallace L, Wang F, Howard-Reed C, Persily A. Contribution of gas and electric stoves to residential ultrafine particle concentrations between 2 and 64 nm: size distributions and emission and coagulation rates. *Environ Sci Tech*. 2008;42:8641-8647.
10. Dennekamp M, Howarth S, Dick C, Cherrie J, Donaldson K, Seaton A. Ultrafine particles and nitrogen oxides generated by gas and electric cooking. *Occup Environ Med*. 2001;58:511-516.
11. Abdullahi KL, Delgado-Saborit JM, Harrison RM. Emissions and indoor concentrations of particulate matter and its specific chemical components from cooking: a review. *Atmos Environ*. 2013;71:260-294.
12. Zhao Y, Zhao B. Emissions of air pollutants from chinese cooking: a literature review. *Build Simul*. 2018;11:977-995.
13. Mohr C, DeCarlo PF, Heringa MF, et al. Identification and quantification of organic aerosol from cooking and other sources in Barcelona using aerosol mass spectrometer data. *Atmos Chem Phys*. 2012;12:1649-1665.
14. Dall'Osto M, Paglione M, Decesari S, et al. On the origin of ams "cooking organic aerosol" at a rural site. *Environ Sci Tech*. 2015;49:13964-13972.
15. Fullana A, Carbonell-Barrachina nA, Sidhu S. Volatile aldehyde emissions from heated cooking oils. *J Sci Food Agr*. 2004;84:2015-2021.
16. Katragadda HR, Fullana A, Sidhu S, Carbonell-Barrachina AA. Emissions of volatile aldehydes from heated cooking oils. *Food Chem*. 2010;120:59-65.
17. Alves CA, Evtyugina M, Cerqueira M, Nunes T, Duarte M, Vicente E. Volatile organic compounds emitted by the stacks of restaurants. *Air Qual Atmos Health*. 2015;8:401-412.
18. Klein F, Platt SM, Farren NJ, et al. Characterization of gas-phase organics using proton transfer reaction time-of-flight mass spectrometry: cooking emissions. *Environ Sci Tech*. 2016;50:1243-1250.
19. Klein F, Farren NJ, Bozzetti C, et al. Indoor terpene emissions from cooking with herbs and pepper and their secondary organic aerosol production potential. *Sci Rep*. 2016;6:36623.
20. Liu T, Liu Q, Li Z, et al. Emission of volatile organic compounds and production of secondary organic aerosol from stir-frying spices. *Sci Tot Environ*. 2017;599:1614-1621.
21. Nazaroff WW, Weschler CJ. Cleaning products and air fresheners: exposure to primary and secondary air pollutants. *Atmos Environ*. 2004;38:2841-2865.
22. Ahn JH, Kim KH, Kim YH, Kim BW. Characterization of hazardous and odorous volatiles emitted from scented candles before lighting and when lit. *J Hazard Mater*. 2015;286:242-251.
23. Haghighat F, Huang H, Lee CS. Modeling approaches for indoor air voc emissions from dry building materials–a review. *ASHRAE Trans*. 2005;111:635-645.
24. National Research Council. *Measuring Exposures and Assessing Health Effects Report*. Washington, DC: National Academy Press; 1986.
25. Matysik S, Ramadan AB, Schlink U. Spatial and temporal variation of outdoor and indoor exposure of volatile organic compounds in Greater Cairo. *Atmos Pollut Res*. 2010;1:94-101.
26. Dodson RE, Houseman EA, Levy JI, Spengler JD, Shine JP, Bennett DH. Measured and modeled personal exposures to and risks from volatile organic compounds. *Environ Sci Tech*. 2007;41:8498-8505.
27. Capello F, Gaddi AV. *Clinical Handbook of Air Pollution-Related Diseases*. Cham, Switzerland: Springer International Publishing; 2018.
28. Kroll JH, Seinfeld JH. Chemistry of secondary organic aerosol: formation and evolution of low-volatility organics in the atmosphere. *Atmos Environ*. 2008;42:3593-3624.
29. Sarwar G, Corsi R, Allen D, Weschler C. The significance of secondary organic aerosol formation and growth in buildings: experimental and computational evidence. *Atmos Environ*. 2003;37:1365-1381.
30. Sarwar G, Corsi R. The effects of ozone/limonene reactions on indoor secondary organic aerosols. *Atmos Environ*. 2007;41:959-973.
31. Coleman BK, Lunden MM, Destaillats H, Nazaroff WW. Secondary organic aerosol from ozone-initiated reactions with terpene-rich household products. *Atmos Environ*. 2008;42:8234-8245.
32. Chen X, Hopke PK. A chamber study of secondary organic aerosol formation by limonene ozonolysis. *Indoor Air*. 2010;20:320-328.
33. Waring MS, Wells JR, Siegel JA. Secondary organic aerosol formation from ozone reactions with single terpenoids and terpenoid mixtures. *Atmos Environ*. 2011;45:4235-4242.
34. Waring MS. Secondary organic aerosol in residences: predicting its fraction of fine particle mass and determinants of formation strength. *Indoor Air*. 2014;24:376-389.
35. Waring MS, Wells JR. Volatile organic compound conversion by ozone, hydroxyl radicals, and nitrate radicals in residential indoor air: magnitudes and impacts of oxidant sources. *Atmos Environ*. 2015;106:382-391.
36. Schauer JJ, Kleeman MJ, Cass GR, Simoneit BRT. Measurement of emissions from air pollution sources. 1. C-1 through C-29 organic compounds from meat charbroiling. *Environ Sci Tech*. 1999;33:1566-1577.

37. Schauer JJ, Kleeman MJ, Cass GR, Simoneit BRT. Measurement of emissions from air pollution sources. 4. C-1-C-27 organic compounds from cooking with seed oils. *Environ Sci Tech*. 2002;36:567-575.
38. Kim KH, Pandey SK, Kabir E, Susaya J, Brown RJ. The modern paradox of unregulated cooking activities and indoor air quality. *J Hazard Mat*. 2011;195:1-10.
39. Wallace LA, Ott WR, Weschler CJ. Ultrafine particles from electric appliances and cooking pans: experiments suggesting desorption/nucleation of sorbed organics as the primary source. *Indoor Air*. 2015;25:536-546.
40. Peng CY, Lan CH, Lin PC, Kuo YC. Effects of cooking method, cooking oil, and food type on aldehyde emissions in cooking oil fumes. *J Hazard Mat*. 2017;324:160-167.
41. Lunden MM, Delp WW, Singer BC. Capture efficiency of cooking-related fine and ultrafine particles by residential exhaust hoods. *Indoor Air*. 2015;25:45-58.
42. Singer BC, Delp WW, Price P, Apte M. Performance of installed cooking exhaust devices. *Indoor Air*. 2012;22:224-234.
43. Nazaroff WW, Cass GR. Mathematical modeling of chemically reactive pollutants in indoor air. *Environ Sci Tech*. 1986;20:924-934.
44. Sparks L, Tichenor B, Chang J, Guo Z. Gas-phase mass transfer model for predicting volatile organic compound (voc) emission rates from indoor pollutant sources. *Indoor Air*. 1996;6:31-40.
45. Chen F, Simon C, Lai AC. Modeling particle distribution and deposition in indoor environments with a new drift–flux model. *Atmos Environ*. 2006;40:357-367.
46. Kraenzmer M. Modeling and continuous monitoring of indoor air pollutants for identification of sources and sinks. *Environ Interact*. 1999;25:541-551.
47. Platt SM, El HaddadI,Pieber SM, et al. Two-stroke scooters are a dominant source of air pollution in many cities. *Nat Commun*. 2014;5:3749.
48. Platt SM, El Haddad I, Pieber SM, et al. Gasoline cars produce more carbonaceous particulate matter than modern filter-equipped diesel cars. *Sci Rep*. 2017;7:4926.
49. Barmet P, Dommen J, DeCarlo PF, et al. OH clock determination by proton transfer reaction mass spectrometry at an environmental chamber. *Atmos Meas Tech*. 2012;5:647-656.
50. Jordan A, Haidacher S, Hanel G, et al. A high resolution and high sensitivity proton-transfer-reaction time-of-flight mass spectrometer (PTR-TOF-MS). *Int J Mass Spectrom*. 2009;286:122-128.
51. Williams LR, Gonzalez LA, Peck J, et al. Characterization of an aerodynamic lens for transmitting particles greater than 1 micrometer in diameter into the Aerodyne aerosol mass spectrometer. *Atmos Meas Tech*. 2013;6:3271-3280.
52. DeCarlo PF, Kimmel JR, Trimborn A, et al. Field-deployable, high-resolution, time-of-flight aerosol mass spectrometer. *Anal Chem*. 2006;78:8281-8289.
53. European Commission. *Manual of Standard Building Specifications*, *Report*. Brussels: Office for infrastructure and logistics, 2011.
54. Eurostat. *Household Composition*, *Poverty and Hardship Across Europe*, *Report*. Luxembourg: Publications Office of the European Union, 2013.
55. Hodgson A, Ming K, Singer B. *Quantifying Object and Material Surface Areas in Residences. Lbnl Report 56786. Report*. Berkeley, CA: Lawrence Berkeley National Laboratory; 2004.
56. Weisel CP, Zhang J, Turpin BJ, et al. Relationships of Indoor, Outdoor, and Personal Air (RIOPA). Part I. Collection methods and descriptive analyses. *Res Rep Health Eff Inst*. 2005;130:1-107.
57. Lee K, Vallarino J, Dumyahn T, Ozkaynak H, Spengler JD. Ozone decay rates in residences. *J Air Waste Manag Assoc*. 1999;49:1238-1244.
58. Morrison G, Shaughnessy R, Shu S. Setting maximum emission rates from ozone emitting consumer appliances in the United States and Canada. *Atmos Environ*. 2011;45:2009-2016.
59. Spicer CW, Kenny DV, Ward GF, Billick IH. Transformations, lifetimes, and sources of NO_2, HONO, and HNO_3 in indoor environments. *Air Waste*. 1993;43:1479-1485.
60. Alvarez EG, Amedro D, Afif C, et al. Unexpectedly high indoor hydroxyl radical concentrations associated with nitrous acid. *Proc Natl Acad Sci USA* 2013;110:13294-13299.
61. AQS data mart. http://www.epa.gov/ttn/airs/airsaqa/detaildata/downloadaqsdata.html, 2013. Accessed: 2016-12-12.
62. USBC. *American Housing Survey. Report*, Washington, DC: US Bureau of the Census, 2016.
63. of Como T, Parzen J, Barzini S. *The Art of Cooking: The First Modern Cookery Book*, 1 edition, Berkeley, CA: University of California Press, 2005.
64. Statista. Number of hours spent cooking per week among consumers worldwide as of June 2014, by country. https://www.statista.com/statistics/420719/time-spent-cooking-per-week-among-consumers-by-country. Accessed: 2016-12-12.
65. FAO. *FAOSTAT Statistical Database: Current Worldwide Annual Meat Consumption per Capita*, *Livestock and Fish Primary Equivalent. Report*, Rome: Food and Agriculture Organization of the United Nation, 2013.
66. Buzby JC, Wells HF, Axtman et al.*Supermarket Loss Estimates for Fresh Fruit*, *Vegetables*, *Meat*, *Poultry*, *and Seafood and Their use in the ERS Loss-Adjusted Food Availability Data*. report. Washington, DC: United States Department of Agriculture, Economic Research Service, 2009.
67. Muth MK, Karns SA, Nielsen SJ, Buzby JC, Wells HF. *Consumer-Level Food Loss Estimates and Their Use in the ERS Loss-Adjusted Food Availability Data*. Washington, DC: United States Department of Agriculture, Economic Research Service. 2011.
68. USDA. *Food Availability (per Capita) Data System. Report*, Washington, DC: United States Department of Agriculture, Economic Research Service, 2016.
69. Elmadfa I. *European Nutrition and Health Report 2009*. report, Vienna: Karger Medical and Scientific Publishers, 2009.
70. State of the plate, 2015 study on america's consumption of fruit and vegetables, produce for better health foundation. http://www.Foundation.org, 2015. Accessed: 2016-12-12.
71. European Spice Association (ESA). *Representing the European Spice and Seasoning Industry*. report, Bonn: European Spice Association, 2015.
72. Thatcher TL, Lai AC, Moreno-Jackson R, Sextro RG, Nazaroff WW. Effects of room furnishings and air speed on particle deposition rates indoors. *Atmos Environ*. 2002;36:1811-1819.
73. Atkinson R, Arey J. Atmospheric degradation of volatile organic compounds. *Chem Rev*. 2003;103:4605-4638.
74. Linstrom PJ, Mallard WG, eds. *NIST Chemistry WebBook*, *NIST Standard Reference Database Number 69*. Gaithersburg, MD: National Institute of Standards and Technology; 2016.
75. Grosjean D, Grosjean E, Williams EL. Rate constants for the gas-phase reactions of ozone with unsaturated alcohols, esters, and carbonyls. *Int J Chem Kinet*. 1993;25:783-794.
76. Colmán EG, Blanco MB, Barnes I, Teruel MA. Ozonolysis of a series of C7–C9 unsaturated biogenic aldehydes: reactivity study at atmospheric pressure. *RSC Adv*. 2015;5:30500-30506.
77. Grosjean D. Atmospheric chemistry of toxic contaminants. 3. Unsaturated aliphatics: Acrolein, acrylonitrile, maleic anhydride. *J Air Waste Manag Assoc*. 1990;40:1664-1669.
78. Bowman JH, Barket DJ, Shepson PB. Atmospheric chemistry of nonanal. *Environ Sci Tech*. 2003;37:2218-2225.
79. Gao T, Andino JM, Rivera CC, Márquez MF. Rate constants of the gas-phase reactions of OH radicals with trans-2-hexenal, trans-2-octenal, and trans-2-nonenal. *Int J Chem Kinet*. 2009;41:483-489.
80. Stephens B, Gall ET, Siegel JA. Measuring the penetration of ambient ozone into residential buildings. *Environ Sci Tech*. 2011;46:929-936.

81. Coleman BK, Morrison GC, Wells J. Kinetics and reaction products of ozone and surface-bound squalene. *J ASTM Int*. 2008;5:1-12.
82. Waring MS, Siegel JA. Indoor secondary organic aerosol formation initiated from reactions between ozone and surface-sorbed d-limonene. *Environ Sci Tech*. 2013;47:6341-6348.
83. Weschler CJ. Ozone in indoor environments: concentration and chemistry. *Indoor Air*. 2000;10:269-288.
84. Carslaw N. A new detailed chemical model for indoor air pollution. *Atmos Environ*. 2007;41:1164-1179.
85. Weschler CJ, Shields HC. Production of the hydroxyl radical in indoor air. *Environ Sci Tech*. 1996;30:3250-3258.
86. Logue J, McKone T, Sherman M, Singer B. Hazard assessment of chemical air contaminants measured in residences. *Indoor Air*. 2011;21:92-109.
87. Zhang J, Zhang J, Chen Q, Yang X. A critical review on studies of volatile organic compound (VOC) sorption by building materials. *ASHRAE Transac*. 2002;108:162.
88. Mendez M, Blond N, Blondeau P, Schoemaecker C, Hauglustaine DA. Assessment of the impact of oxidation processes on indoor air pollution using the new time-resolved INCA-indoor model. *Atmos Environ*. 2015;122:521-530.
89. Lide DR *CRC Handbook of Chemistry and Physics* (Vol. 85). Boca Raton, FL: CRC Press; 2004.
90. An Y, Zhang J, Shaw C. Measurements of VOC adsorption/desorption characteristics of typical interior building materials. *HVAC Res*. 1999;5:297-316.
91. Singer BC, Revzan KL, Hotchi T, Hodgson AT, Brown NJ. Sorption of organic gases in a furnished room. *Atmos Environ*. 2004;38:2483-2494.
92. Singer BC, Pass RZ, Delp WW, Lorenzetti DM, Maddalena RL. Pollutant concentrations and emission rates from natural gas cooking burners without and with range hood exhaust in nine california homes. *Build Environ*. 2017;122:215-229.
93. Singer BC, Hodgson AT, Hotchi T, et al. Sorption of organic gases in residential rooms. *Atmos Environ* 2007;41:3251-3265.
94. Loza CL, Craven JS, Yee LD, et al. Secondary organic aerosol yields of 12-carbon alkanes. *Atmos Chem Phys*. 2014;14:1423-1439.
95. Chacon-Madrid H, Donahue N. Fragmentation vs. functionalization: chemical aging and organic aerosol formation. Atmos. *Chem Phys*. 2011;11:10553-10563.
96. Hu T, Singer BC, Logue JM. *Compilation of Published PM2. 5 Emission Rates for Cooking, Candles and Incense for use in Modeling of Exposures in Residences*. Technical report, Berkeley, CA: Lawrence Berkeley National Lab. (LBNL); 2012.
97. Seaman VY, Bennett DH, Cahill TM. Origin, occurrence, and source emission rate of acrolein in residential indoor air. *Environ Sci Tech*. 2007;41:6940-6946.
98. Fountoukis C, Megaritis AG, Skyllakou K, et al. Simulating the formation of carbonaceous aerosol in a European megacity (Paris) during the MEGAPOLI summer and winter campaigns. *Atmos Chem Phys*. 2016;16:3727-3741.
99. Ots R, Vieno M, Allan JD, et al. Model simulations of cooking organic aerosol (COA) over the UK using estimates of emissions based on measurements at two sites in London. *Atmos Chem Phys*. 2016;16:13773-13789.
100. Reyes-Villegas E, Bannan T, Le Breton M, et al. Online chemical characterization of food-cooking organic aerosols: implications for source apportionment. *Environ Sci Tech*. 2018;52:5308-5318.
101. Huang RJ, Wang Y, Cao J, et al. Primary emissions versus secondary formation of fine particulate matter in the most polluted city (Shijiazhuang) in North China. *Atmos Chem Phys*. 2019;19:2283-2298.
102. Robinson ES, Gu P, Ye Q, et al. Restaurant impacts on outdoor air quality: elevated organic aerosol mass from restaurant cooking with neighborhood-scale plume extents. *Environ Sci Tech*. 2018;52:9285-9294.
103. Elser M, El Haddad I, Maasikmets M, et al. High contributions of vehicular emissions to ammonia in three european cities derived from mobile measurements. *Atmos Environ*. 2018;175:210-220.
104. Shu S, Morrison GC. Surface reaction rate and probability of ozone and alpha-terpineol on glass, polyvinyl chloride, and latex paint surfaces. *Environl Sci Tech*. 2011;45:4285-4292.
105. Seaman VY, Bennett DH, Cahill TM. Indoor acrolein emission and decay rates resulting from domestic cooking events. *Atmos Environ*. 2009;43:6199-6204.
106. Hussein T, Glytsos T, Ondráček J, et al. Particle size characterization and emission rates during indoor activities in a house. *Atmos Environ*. 2006;40:4285-4307.
107. Levy J, Dumyahn T, Spengler J. Particulate matter and polycyclic aromatic hydrocarbon concentrations in indoor and outdoor microenvironments in Boston, Massachusetts. *J Expo Anal Environ Epid*. 2002;12:104-114.
108. See SW, Balasubramanian R. Physical characteristics of ultrafine particles emitted from different gas cooking methods. *Aerosol Air Qual Res*. 2006;6:82-92.
109. See S, Balasubramanian R. Chemical characteristics of fine particles emitted from different gas cooking methods. *Atmos Environ*. 2008;42:8852-8862.
110. Buonanno G, Morawska L, Stabile L. Particle emission factors during cooking activities. *Atmos Environ*. 2009;43:3235-3242.
111. Gilbert NL, Guay M, Miller JD, Judek S, Chan CC, Dales RE. Levels and determinants of formaldehyde, acetaldehyde, and acrolein in residential indoor air in Prince Edward Island, Canada. *Environ Res*. 2005;99:11-17.
112. Huang Y, Ho SSH, Ho KF, Lee SC, Yu JZ, Louie PKK. Characteristics and health impacts of VOCs and carbonyls associated with residential cooking activities in Hong Kong. *J Hazard Mater*. 2011;186:344-351.
113. Rey deCastro B. Acrolein and asthma attack prevalence in a representative sample of the United States adult population 2000–2009. *PLoS One*. 2014;9:e96926.
114. Jurvelin JA, Edwards RD, Vartiainen M, Pasanen P, Jantunen MJ. Residential indoor, outdoor, and workplace concentrations of carbonyl compounds: relationships with personal exposure concentrations and correlation with sources. *J Air Waste Manag Assoc*. 2003;53:560-573.
115. Liu W, Zhang J, Zhang L, et al. Estimating contributions of indoor and outdoor sources to indoor carbonyl concentrations in three urban areas of the United States. *Atmos Environ*. 2006;40:2202-2214.
116. Hippelein M. Background concentrations of individual and total volatile organic compounds in residential indoor air of Schleswig-Holstein, Germany. *J Environ Monit*. 2004;6:745-752.
117. Edwards RD, Jurvelin J, Saarela K, Jantunen M. VOC concentrations measured in personal samples and residential indoor, outdoor and workplace microenvironments in EXPOLIS-Helsinki, Finland. *Atmos Environ*. 2001;35:4531-4543.

SUPPORTING INFORMATION

Additional supporting information may be found online in the Supporting Information section at the end of the article.

How to cite this article: Klein F, Baltensperger U, Prévôt ASH, El Haddad I. Quantification of the impact of cooking processes on indoor concentrations of volatile organic species and primary and secondary organic aerosols. *Indoor Air*. 2019;29:926–942. https://doi.org/10.1111/ina.12597